Engineering Science and Technology, an International Journal 24 (2021) 158–170

HOSTED BY

ELSEVIER

Contents lists available at ScienceDirect

Engineering Science and Technology, an International Journal

journal homepage: www.elsevier.com/locate/jestch

Full Length Article

A novel unified maximum power extraction framework for PMSG based WECS using chaotic particle swarm optimization derivatives

Emre Hasan Dursun, Hasan Koyuncu, Ahmet Afsin Kulaksiz *

Department of Electrical and Electronics Engineering, Faculty of Engineering and Natural Sciences, Konya Technical University, Konya, Turkey

ARTICLE INFO

Article history:
Received 6 March 2020
Revised 11 May 2020
Accepted 15 May 2020
Available online 29 May 2020

Keywords:
Chaos based optimization
Fast terminal sliding mode control
Maximum power point tracking
Permanent magnet synchronous generator
Wind energy conversion system

ABSTRACT

The most important issue in the use of wind energy conversion systems (WECS) is to ensure maximum power extraction for attaining increased efficiency. In this study, maximum power extraction frameworks operating the state-of-the-art optimization methods are presented for permanent magnet synchronous generator (PMSG) based WECS. These frameworks consist of a fast terminal sliding mode control (FTSMC) based MPPT controller and a hybrid MPPT approach that combines chaotic based particle swarm optimization (PSO) derivatives and optimal relation based (ORB) method. Chaotic dynamic weight PSO (CDW-PSO) and Gauss map based chaotic PSO (GM-CPSO), which are remarkable and recent optimization techniques, are utilized to achieve optimum coefficients to ensure efficient MPPT operation. After acquiring the optimum coefficients, the framework passes to ORB operation part. Moreover, the proposed frameworks track extracted power within certain limits during the operation of WECS and make transition between the best coefficients if necessary. On the other hand, FTSMC is used to track the MPPT references that are determined via hybrid MPPT algorithms. To validate the proposed frameworks, they are tested in Matlab/Simulink environment for three specific wind speed scenarios. GM-CPSO based ORB and CDW-PSO based ORB MPPT methods are compared with ORB and tip speed ratio (TSR) methods under these scenarios. Consequently, it is revealed that proposed methods contribute to MPPT efficiency by providing higher power extraction than other conventional methods.

1. Introduction

The conventional energy resources have low efficiency, are becoming insufficient, and causes some threats such as pollution and global warming [1]. In recent years, these threats decreasing their usability have necessitated countries to seek renewable energy-based power generation systems [2]. As the wind energy is clean, infinite and reliable, it grows much faster and attracts a lot of attention by researchers and investors [3,4]. Moreover, as it can reduce the cost of power generation, efficient usage of wind energy can obviously have a vital role in meeting growing energy demand.

In literature studies and industrial applications, Wind Energy Conversion Systems (WECSs) have a special place in generating electrical power from wind power. WECSs generally comprise of wind turbine, generator, power converter and its controller [5]. In addition, there is a need for more effective and innovative control strategies and algorithms in order to improve capabilities such as power conversion quality and efficiency for WECSs [6].

WECSs can be divided into two main types as constant-speed (CS-WECS) and variable-speed (VS-WECS). CS-WECS has simple design but low efficiency since it can be operated in a narrow wind speed range [7]. However, as the wind owns a random nature and its speed varies depending on the conditions, the power of wind turbine is always fluctuating [4]. In addition, maximum power must be captured at each wind speed as much as possible, and this can only be carried out with MPPT operation in the VS-WECS [4,8]. VS-WECS configurations range from small-scale stand-alone structures to high-powered wind farms [9], and two different power converter topologies are commonly encountered: back-to-back converter (BTBC) and rectifier-boost converter [10,11]. Although BTBC topology is more advantageous for high-power WECS, the latter one is more preferred in terms of efficiency and cost for small-scale applications. Besides, it offers a very good alternative to rural areas remote to grid network.

Squirrel cage induction generators (SCIGs) [12], doubly-fed induction generators (DFIGs) [13] and permanent magnet synchronous generators (PMSGs) [4,6,7] are used to convert the

* Corresponding author at: Konya Technical University, Engineering and Natural Sciences, Department of Electrical and Electronics Engineering, Selcuklu, Konya, Turkey.

E-mail address: aakulaksiz@ktun.edu.tr (A.A. Kulaksiz).

Peer review under responsibility of Karabuk University.

https://doi.org/10.1016/j.jestch.2020.05.005
2215-0986/

Nomenclature

List of symbols

P_m	Mechanical power
ρ_a	Air density (kg/m^3)
A	Swept area of turbine blades (m^2)
C_P (λ, β)	Power coefficient
λ	Tip speed ratio
β	Pitch angle
R	Turbine blade radius (m)
v_w	Wind speed (m/s)
η_{gen}	generator efficiency
η_{conv}	converter efficiency
ω_m	turbine rotor angular speed
k_v	approximation constant
P_L	electrical power delivered to the load
V_{DC}	rectified voltage
K_{opt}	optimum coefficient
u,u	the switching control function, its inverse logic
κ	feedback converter ratio
I_{DC}, I_O	BC input current, BC output current
V_O	BC output voltage
p, q	positive odd integers
s	sliding mode manifold
u_{eq}, u_{sw}, u_t	equivalent, switching, total control signal
K_{sw}	coefficient
R,L,C	Resistor, inductor, capacitor
α,γ	Independent coefficient of sliding manifold
$X_1, X_2, \dot{X}_2$	controlled system variables
$V_i(t)$	current velocity vector of ith particle
$V_i(t+1)$	new velocity vector of ith particle
$X_i(t)$	current position vector of ith particle
$X_i(t+1)$	new position vector of ith particle
ω	inertia weight for optimization methods
c_1, c_2	acceleration constants
X_{min},X_{max}	position limitations
V_{min},V_{max}	velocity limitations
$X_{pbest(i)}(t)$	individual best position of ith particle
$X_{gbest}(t)$	global best solution of the whole swarm
$f(i)$	fitness value at the ith iteration dynamic weights
$w_i = \psi$, w_i'	dynamic weights
ρ	a random number within the range (0,1)
$r_1(t)$, $r_2(t)$	random numbers within the range (0,1)

List of abbreviations

BC	Boost converter
BTBC	Back-to-back converter
CDW-PSO	Chaotic dynamic weight PSO
CKH	Chaotic krill herd
CS-WECS	Constant-Speed WECS
DFIG	Doubly-fed induction generator
DW-PSO	Dynamic weight PSO
FLC	Fuzzy logic control
FTSMC	Fast terminal sliding mode control
GM-CPSO	Gauss map based chaotic PSO
HCS	Hill climbing search
INC	Incremental conductance
KH	Krill herd
MPPT	Maximum power point tracking
NN	Neural network
ORB	Optimum relation based
OTC	Optimal torque control
PMSG	Permanent magnet synchronous generator
PSF	Power signal feedback
PSO	Particle swarm optimization
SCIG	Squirrel cage induction generator
SMC	Sliding mode control
SM-PSO	Sine map based chaotic PSO
TSR	Tip speed ratio
VS-WECS	Variable-Speed WECS
WECS	Wind Energy Conversion System

mechanical energy of turbine into electrical form. While DFIGs are preferred in high-power installations, PMSGs are distinguished by several advantages such as high power density, high efficiency and reliability, low maintenance cost and direct-driven operation capability in small and medium sized applications [14,15]. For this reason, in this study, the authors prefer PMSG based VS-WECS configuration that consists of rectifier and DC-DC boost converter.

Although it is plentiful in suitable regions, the wind speed is of highly random and time-varying nature. On the other hand, for each wind speed, there is a unique operating point where maximum power can be captured. To this end, MPPT operation should be ensured in the range between cut-in and rated wind speed in order to maximize the power.

In the literature, MPPT operation is examined in two categories: 1) MPPT search methods to determine the optimal operating point, 2) Controller designs to bring the WECS to this optimal point. As these two categories will affect the overall system efficiency, both are vital and extensive researches have been carried out on them.

In some literature studies; various methods were used as MPPT controller. PI and PID type classical controllers are easy to design and its parameters can be sometimes optimized to improve dynamical performance by different optimization techniques [16,17]. However, these methods cannot present sufficient performance in many applications that includes strong nonlinearity caused by wind turbines aerodynamics, power converters, besides the nature of wind flow [18]. Therefore, some of the more advanced methods, for instance, Fuzzy Logic Control (FLC) [11], back-stepping [19] and different sliding mode control (SMC) techniques [6,20] have been used in the WECS by researchers. In this study, fast terminal sliding mode controller (FTSMC), which is capable of fast convergence and better performance by removing the disadvantages of conventional SMC [21], is designed as a voltage regulator to generate the switching signal of power converter for bringing the system into the operating point determined by MPPT method.

Either new, modified, or hybrid, various MPPT methods have been proposed in the literature. However, they have their own merit and demerits in terms of requirement of mechanical sensor and preliminary information, process load, complexity and convergence speed [1,14]. The most common methods are hill-climbing search (HCS) [22], incremental conductance (INC), optimal torque control (OTC) [23], tip speed ratio (TSR) [24], power signal feedback (PSF) and optimal relation based (ORB) method [25]. TSR method is relatively simple which aims to maximize C_P by keeping the system in λ_{opt}. Nevertheless, it needs wind speed information. Whilst PSF method does not need to measure wind speed, it is necessary to obtain the characteristic curve of the WECS, that is, turbine power curve *vs.* shaft speed by making off-line experiments. OTC method is one of the basic methods trying to adjust the generator torque to the reference torque in which it will reach

maximum power at a specific wind speed. However, in case high wind turbulences occur, its performance deteriorates and the efficiency of OTC remains relatively lower than TSR. HCS is an economical and simple method where peak search of the output power is performed by measuring and perturbing the generator speed. Although the output power is usually searched with constant step changes, some studies on variable step-size have also been fulfilled. In addition, optimal adjustment of step-size creates a challenging subject. ORB is operated with optimum relations between different system parameters without wind speed sensor and then MPPT references are calculated in advance and generally stored in the look-up table. Furthermore, its response to wind speed change is fast and it has ease of application. The optimum coefficient K_{opt} values can be calculated with regard to the defined relation, however, the accurate determination of coefficients is challenging since they vary for each unique wind speed. At this point, optimization techniques can offer a solution to determine K_{opt} values without any wind speed measurement. One essential objective of this paper is to find a promising solution to this issue.

Stochastic behavior is utilized in various themes like numerical function optimization, hybrid classifier design, and pattern recognition [26,27]. The convergence of methods is proposed to be efficient for the handled fitness function, and this process should be realized with influential methods to achieve remarkable performance. There exists various strategies of particle swarm optimization (PSO) considering different derivatives to provide better convergence than other techniques. One of which expressed in [28] proposed two efficient derivatives of PSO that are Sine map based chaotic PSO (SM-CPSO) and dynamic weight PSO (DW-PSO). By combining SM-CPSO and DW-PSO algorithms, chaotic dynamic weight PSO (CDW-PSO) was generated to design a robust structure. On numerical function optimization, CDW-PSO surpassed twenty optimization algorithms including basic methods, chaotic approaches, PSO based derivatives and state-of-the-art studies. In [28], Sine map was evaluated to update the inertia weight of PSO according to its usage in krill herd (KH) and chaotic krill herd (CKH) algorithms [29,30]. However, PSO involves different dynamics (formulations and phenomena) inside, and the necessary map can vary from one method to another. With this inspiration, Koyuncu [26] examined ten chaotic maps in PSO to reveal whether chaotic maps are essential in the update of inertia weight or not. In the first part of experiments, the CPSOs including ten chaotic maps are compared with each other beside general PSO. Thus, it arose that Gauss map based CPSO (GM-CPSO) was the only one outperforming general PSO in every condition and was also the best one among all CPSOs. In the second part, GM-CPSO was compared with SM-CPSO, DW-PSO and CDW-PSO methods in different dimensional conditions. GM-CPSO outrivaled SM-CPSO and DW-PSO approaches on global optimization of benchmark functions. Herein, GM-CPSO can be seen as a part inside of CDW-PSO. However, the performances obtained by CDW-PSO and GM-CPSO methods were so close that, the third experiment was considered to objectively arise the best one. Epileptic seizure recognition was implemented using neural network (NN) based hybrid classifiers that contain the best three methods (DW-PSO, CDW-PSO, GM-CPSO) of the second experiment. GM-CPSO-NN outperformed DW-PSO-NN and CDW-PSO-NN algorithms on detection of seizure *vs.* non-seizure patterns in terms of obtaining reliable performance. Consequently, GM-CPSO proved oneself on global function optimization and pattern recognition as a state-of-the-art method [27].

In this paper, CDW-PSO and GM-CPSO algorithms are handled to design an efficient framework operating hybrid optimization and ORB MPPT method to extract maximum power from WECS.

The intended contributions of this study made to the literature can be seen as follows:

- GM-CPSO and CDW-PSO algorithms have been diversely hybridized with ORB MPPT method to create two effective maximum power extraction framework that has not been used in WECS before. These algorithms provide a solution to obtain K_{opt} coefficients that will ensure MPPT without system parameters. After these coefficients are obtained in this way, ORB operation mode is activated.
- The proposed MPPT framework is mechanically sensorless, has a very fast convergence without the need for any system prior knowledge, and ensures maximum power extraction by switching between the best coefficients and by following the power changes during operation.
- A unified maximum power extraction framework has been created using the FTSMC as a voltage regulator to bring the system to the optimal voltage. Herein, this voltage is determined by the proposed hybrid MPPT for PMSG-based WECS configuration consisting of rectifier and DC-DC boost converter.
- Using three wind speed profiles, proposed methods are analyzed in detail by comparing with ORB and TSR methods, and further improved MPPT efficiency by providing higher power extraction than the others.

The rest of this study is presented as follows: In Section 2, the designed WECS configuration is given in detail. Section 3 presents the state-of-the-art optimization algorithms, MPPT method and FTSMC controller in a comprehensive manner. Simulation results and interpretations are evaluated in Section 4, and concluding remark is given in Section 5.

2. WECS configuration

The schematic diagram of the designed WECS configuration is presented in Fig. 1. Herein, WECS configuration consists of wind turbine, PMSG, three phase uncontrolled rectifier, boost converter (BC), load, and combined maximum power extraction framework. Moreover, it can be seen that the unified framework comprises hybrid optimization, ORB MPPT method, and fast terminal sliding mode MPPT controller.

As seen in Fig. 1, some voltage and current information are measured from WECS. The hybrid MPPT method aims to maximize the electrical power directly on the terminal out, namely on the load, to achieve more accurate results. In addition, while the input of this method is P_O output power, which is obtained by multiplying the output voltage V_O with output current I_O, its output is the optimal operating point V_{in_opt} against the maximum power. Besides, BC input voltage V_{in}, BC output voltage V_O and reference voltage V_{in_opt} are the inputs of FTSMC that are considered as a voltage controller. Whereas, the output of FTSMC can be regarded as the control signal that will bring the WECS to the operating point.

3. Material and methods

In this paper, the proposed framework for extraction of maximum output power focuses on three special topics as optimization algorithms, MPPT methods and MPPT controller. The first one is optimization algorithms, which includes chaotic dynamic weight PSO (CDW-PSO) and gauss map based chaotic PSO (GM-CPSO). The second one is MPPT methods that are mentioned as TSR MPPT, ORB MPPT and Hybrid optimization based ORB methods. The last one is MPPT controller, which deals with the fast terminal sliding mode control method as a voltage regulator to bring the system to the optimal voltage.

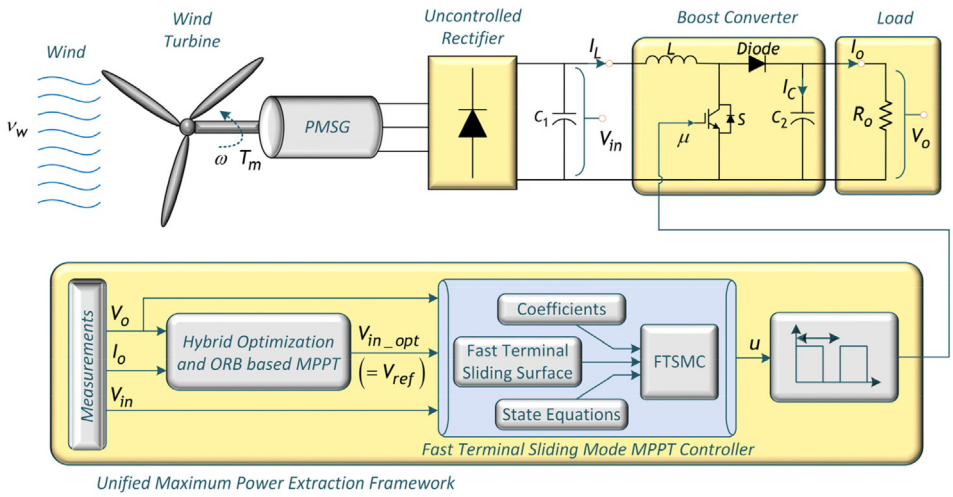

Fig. 1. PMSG based WECS configuration.

3.1. Optimization algorithms

This subsection begins by explaining two state-of-the-art optimization methods, which are utilized to achieve the necessary reference voltage to be used in WECS. Chaotic dynamic weight PSO (CDW-PSO) and Gauss map based chaotic PSO (GM-CPSO) are designed as the modified versions of PSO algorithm. These algorithms have also proved oneself in different disciplines and are also superior to basic optimization methods, chaotic based approaches, and novel optimization techniques. GM-CPSO and CDW-PSO algorithms are applied to the control area firstly in this study.

As in PSO, every solution is named as a *particle* in GM-CPSO and CDW-PSO methods, and each *particle* corresponds to a new *position* covering a dimension equal to the parameters to be optimized. The tradeoff between exploration and exploitation is ensured using the global best solution obtained in the whole swarm and the individual best positions procured of every particle.

3.1.1. Gauss map based chaotic particle swarm optimization

GM-CPSO involves nearly all phenomena in PSO method, with the exception of stable or linear updated inertia weight. As in PSO algorithm, GM-CPSO utilizes velocity and position concepts to provide the convergence towards the global point(s), and are respectively shown in (1) and (2) [26].

$$V_i(t+1) = \omega V_i(t) + c_1 r_1(t)\left(X_{pbest(i)}(t) - X_i(t)\right) + c_2 r_2(t)\left(X_{gbest}(t) - X_i(t)\right) \quad (1)$$

$$X_i(t+1) = X_i(t) + V_i(t+1) \quad (2)$$

In (1) and (2); $V_i(t)$ and $X_i(t)$ respectively symbolize the current velocity and position vectors of ith particle, whilst $V_i(t+1)$ and $X_i(t+1)$ add up to the new ones. $X_{pbest(i)}(t)$ and $X_{gbest}(t)$ specify the individual best position of ith particle and global best solution of the whole swarm. c_1 and c_2 are acceleration constants adjusting the movements to the individual and global best positions and are formulated according to (3) [31]. In the literature, these constants are generally chosen as equal to '2' to acquire better fitness [28]. $r_1(t)$ and $r_2(t)$ are generated in the range of (0,1) and provide diversity to better explore the search space. ω connotes the inertia weight limiting the effect of the current velocity to the step size (new velocity). In GM-CPSO, the arrangement of ω is performed using Gauss (Mouse) map presented in (4) [26,27].

$$c_1 + c_2 \leqslant 4 \quad (3)$$

$$\omega(i+1) = \begin{cases} 1 & \omega(i) = 0 \\ \frac{1}{mod\ (\omega(i),1)} & otherwise \end{cases}, \ \omega(0) = 0.7 \quad (4)$$

In (3), the first assignment of inertia weight is advised as '0.7' to obtain better chaotic behavior [32]. In terms of the presented chaotic behavior, Gauss map can change or eliminate the effect of the current velocity on step size. Even if this process indirectly affects the new position, it improves the searching capability by diversifying the solutions (positions) in search space. Herein, Gauss map induces more variety to guarantee better convergence for optimal solutions [26,27].

The boundaries of velocity values are regulated according to (5). X_{min} and X_{max} are defined as the minimum and maximum values that a position can become, while V_{min} and V_{max} are specified for the velocity limitations. The parameter 'k' is used to connect the velocity boundaries with the position limitations, and a value of '0.2' is assigned as advised in most of PSO based derivatives [26,28].

$$[V_{\min}, V_{\max}] = k * [X_{\min}, X_{\max}] \quad (5)$$

3.1.2. Chaotic dynamic weight particle swarm optimization:

CDW-PSO differentiates from PSO algorithm by handling the dynamic weights for position update and by referring Sine chaotic map for the set of inertia weight. Velocity concept of general PSO is preserved in CDW-PSO algorithm, and it operates (1) to calculate the step size. In (1), all parameter definitions about velocity remain unchanged with GM-CPSO method, except inertia weight (ω) which is tuned using the Sine map defined in (6) [26,28].

$$\omega = x_k = A.\sin(\pi x_{k-1}),\ \{x_k \in (0,1),\ 0 < A \leqslant 1,\ k = 1,2,\ldots,M_{max}\} \quad (6)$$

In (6); k and M_{max} are respectively the current and maximum iteration numbers, and x_k is described as the inertia value at k^{th} iteration. Sine map yields diversity for restriction of step size, however, it can remove the effect of current velocity to step size less than Gauss map. (4) and (6) suggest that this situation is connected with the nature of the utilized chaotic map.

To increase the effect of global best solution directly to the new position, the position concept of CDW-PSO is formulated according to (7). Herein, w_i (ψ) and w_i' are the dynamic weights respectively identified in (8) and (9) [26,28].

$$X_i(t+1) = X_i(t)w_i + V_i(t+1)w_i' + \rho X_{gbest}(t)\psi \quad (7)$$

$$w_i = \psi = \frac{\exp(f(i)/u)}{(1+\exp(-f(i)/u))^{iter}} \tag{8}$$

$$w_i' = 1 - w_i \tag{9}$$

In (7), ψ is assigned as the acceleration constant that is equal to w_i as seen in (8). w_i and w_i' take inversely correlated values according to (9). This condition ($w_i = \psi$) nearly yields mutual increase or decrease for the effect of current position and global best solution to the new position. However, ρ is a random number within the range (0,1) and is added to the formulation to ensure diversity and to restrict the effect of global best position to the new position. On the other hand, the effect of step size on the new position is reverse due to the usage of w_i'. In (8), u and $f(i)$ are respectively the mean of fitness values obtained at the first iteration and the fitness value at the ith iteration.

Dynamic weights are determined according to the fitness values achieved among iterations. As defined in [28], if the fitness of the best particle is large, w_i tends to increase ($w_i'\downarrow$) and the effects of global best and current positions are enhanced on the new position. Contrary to this situation, if the fitness of the best particle is small, it yields bigger w_i' values ($w_i\downarrow$) and the effect of step size is raised. The formation of CDW-PSO and GM-CPSO methods are presented in Fig. 2.

3.2. MPPT methods

This subsection gives a detailed overview of TSR, ORB and proposed MPPT methods to allow making a comparison of their performance.

3.2.1. TSR MPPT method

TSR method aims to keep mechanical power captured from wind turbine at maximum. Wind turbine's mechanical power is as follows [33]:

$$P_m = 0.5\rho_a A C_p(\lambda,\beta) v_w{}^3 \tag{10}$$

where ρ_a is air density, A symbolizes the swept area of turbine, $C_P(\lambda, \beta)$ means the power coefficient of turbine and v_w signifies the wind speed. C_P is a nonlinear function and changes only depending on tip speed ratio (λ) in WECS with fixed-pitch angle. On the other hand, λ depends on shaft and wind speeds which is as follows:

$$\lambda = \frac{R\omega_m}{v_w} \tag{11}$$

where R is the radius of turbine. General formula of C_P can be defined below and C_P *vs.* λ characteristic of WT in this paper is as shown in Fig. 3.

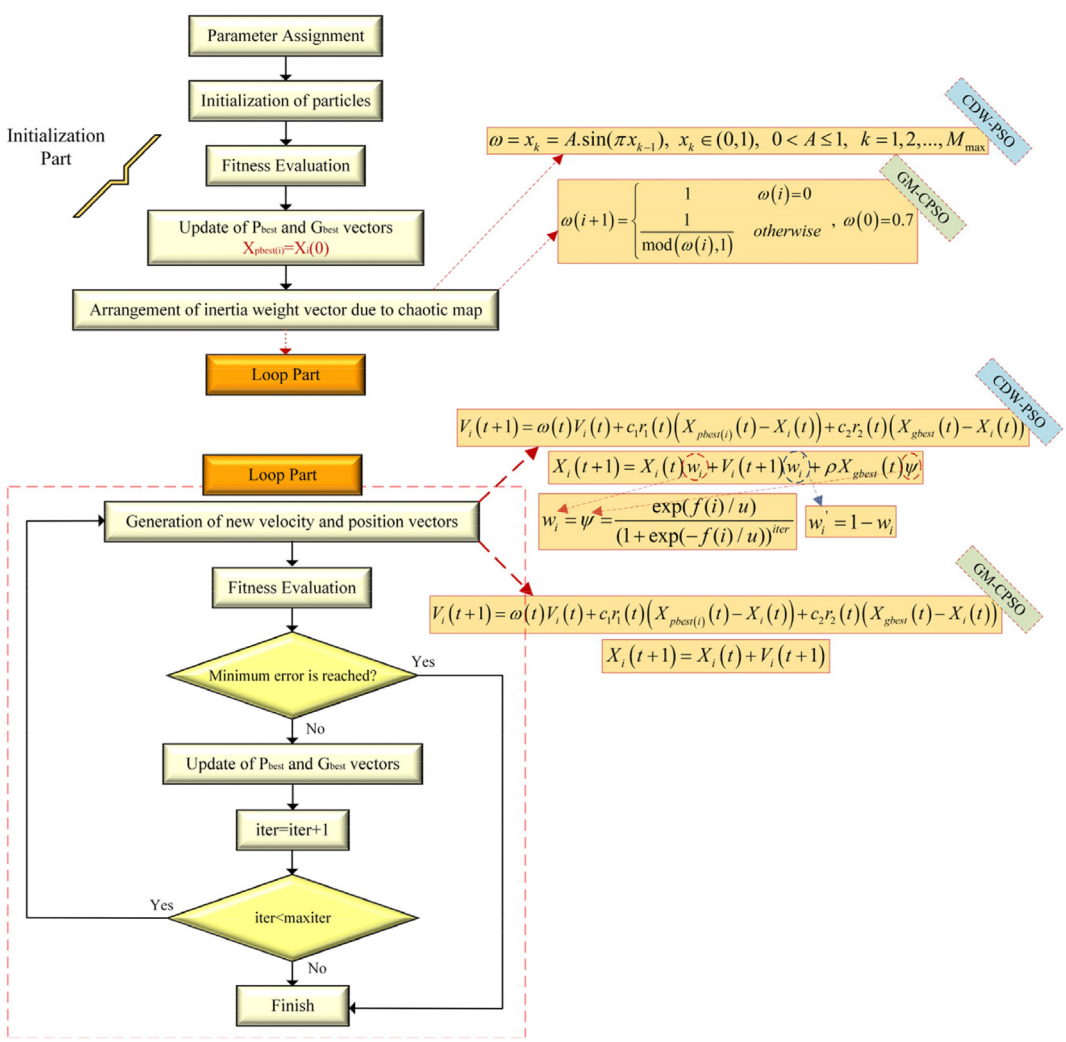

Fig. 2. The formation of CDW-PSO and GM-CPSO methods.

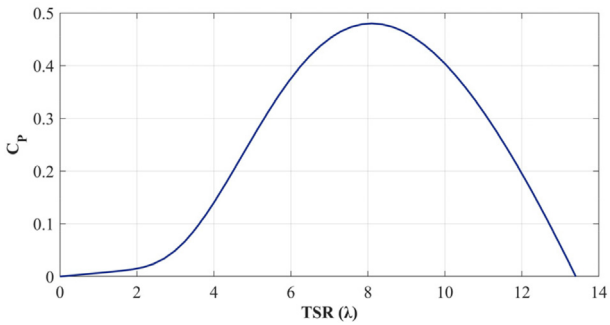

Fig. 3. C_P *vs.* λ characteristic of WT.

$$\begin{cases} C_p(\lambda,\beta) = C_1\left(\frac{C_2}{\lambda_i} - C_3\beta - C_4\right)e^{-(C_5/\lambda_i)} + C_6\lambda \\ \frac{1}{\lambda_i} = \frac{1}{\lambda+0.08\beta} - \frac{0.035}{\beta^3+1} \end{cases} \tag{12}$$

3.2.2. ORB MPPT method

ORB method is operated based on the relation between different system variables. This relation can usually be based on the shaft speed *vs.* power, torque *vs.* power, rectified DC voltage *vs.* power and DC current *vs.* DC voltage in applications [5,34]. In this study, the ORB relation is established between the power on the load and the BC input voltage for efficiency. Definition of this relation can be made theoretically. If v_w is derived from (11) and replaced into (10), the maximum mechanical power is obtained as follows [35]:

$$P_{m\_\max} = 0.5\frac{\rho_a \pi R^5 C_{pmax}}{\lambda_{opt}{}^3}\omega_m{}^3 = K_{p\_opt}\omega_m{}^3 \tag{13}$$

From here, taking into account that the losses in the generator and converter are not constant, the electrical power on the load can be calculated as below:

$$P_L = \eta_{gen}\eta_{conv}P_m \tag{14}$$

where, η_{gen} and η_{conv} express the generator and converter efficiencies, respectively. Furthermore, if the diode losses in the rectifier and convergence at low powers are neglected, the linear relation between rectified voltage V_{DC} and ω_m is as follows:

$$V_{DC} = k_V\omega_m \tag{15}$$

where k_v symbolizes an approximation constant. Here, $P_{L\_\max}$ can be related according to V_{DC}, which is expressed as:

$$P_{L\_max} = \eta_{gen}\eta_{conv}P_m = \eta_{gen}\eta_{conv}K_{p\_opt}\omega_m{}^3 = \therefore = K_{opt}V_{DC\_opt}{}^3 \tag{16}$$

In this way, BC input voltage that will ensure maximum electrical power can be determined without using any mechanical sensor. Herein, optimum coefficient K_{opt} values can be calculated with regard to the defined relation but the accurate assignment of these coefficients seems challenging due to the fact that these vary for each unique wind speed. However, they are obtained by performing simulation tests and validations to operate the ORB and to compare with other approaches.

3.2.3. Hybrid optimization and ORB MPPT method

The drawback of ORB method is the difficulty at the setting of exact K_{opt} coefficients. Thus, hybrid optimization technique is handled with the idea that it can offer a solution by determining these coefficients in order to relate maximum electrical power and DC voltage. The flowchart of hybrid optimization and ORB MPPT framework is demonstrated in Figs. 4 and 5, respectively. It is obvious from Fig. 4 that the algorithm consists of two main parts: 1) Optimization part, 2) ORB part. In the first part, optimization method is operated to obtain optimal relation and determine the V_{DC} voltage, in which the power reaches the maximum value. The solution of optimization technique offers some advantages such as no need to know the system parameters and to operate without a mechanical sensor. Furthermore, maximization is performed with GM-CPSO and CDW-PSO algorithms by keeping the search space and optimization coefficient constant for each one, and these are presented in the flowchart. Herein, when all values are determined, ORB method is operated by switching to the second part. When the second part is examined, it can be seen that a predefined critical power P_{th} is determined. If a change in the extracted maximum power during the operation occurs, this algorithm detects a change in the wind speed by tracking power and the difference at power. Thus, with the consideration that maximum power can be reached at another reference value, it makes transitions between optimum coefficients. Then, the operating point V_{ref} is determined based on this coefficient and transferred to the controller so that the maximum power can be ensured. If it remains below the critical level, no changes are made and current reference voltage for the same K_{opt} is transferred to the controller.

3.3. Fast terminal sliding mode controller

A DC-DC boost converter illustrated in Fig. 1 is used in the power converter of the WECS. Since the boost converter consists of diode, inductor, capacitor and power switching element, it is considerably nonlinear and variable by nature. Successful MPPT performances with traditional control techniques cannot be achieved in such a completely nonlinear system [6]. Therefore, FTSMC is designed as voltage regulator here. Also, this control method offers fast dynamic response, high stability and robustness for parametric uncertainties during the operation over a wide range of wind speed.

To design the fast terminal sliding mode voltage controller, the behavior model of boost converter is firstly examined, which is as follows [36,37]:

$$\begin{cases} \frac{dV_o}{dt} = \bar{u}\,\frac{I_L}{C} - \frac{V_o}{RC} \\ \frac{dI_L}{dt} = -\bar{u}\,\frac{V_o}{L} + \frac{V_{in}}{L} \\ I_C = \bar{u}\,I_L - \frac{V_o}{R} \\ V_{in} = \kappa V_o \quad , \ \{\kappa = 1-d\} \end{cases} \tag{17}$$

where, u and $\bar{u}$ are the switching control function and its inverse logic, respectively. Also, κ indicates feedback converter ratio. I_{DC}, I_O and V_O respectively denote BC input current, BC output current, and output voltage.

The controlled system variables are given below [38]:

$$\begin{cases} X_1 = V_{in\_opt} - V_{in} \\ X_2 = \kappa\left(\frac{V_o}{RC} + \int \bar{u}\,\frac{V_o - V_{in}}{LC}dt\right) \\ \dot{X}_2 = -\frac{X_2}{RC} + \bar{u}\,\kappa\left(\frac{V_o - V_{in\_opt} + X_1}{LC}\right) \end{cases} \tag{18}$$

The sliding mode manifold is selected as follows [39]:

$$s = \dot{X}_1 + \alpha X_1 + \gamma X_1{}^{p/q} \tag{19}$$

where α *and* γ are independent coefficient of manifold. Also, p and q are positive odd integer and $0.5 < p/q < 1$. If it is defined as $\theta = p/q$ and taking the derivate with respect to time, it yields:

$$\dot{s} = \ddot{X}_1 + \alpha\dot{X}_1 + \gamma\theta|X_1|^{\theta-1}\dot{X}_1 \tag{20}$$

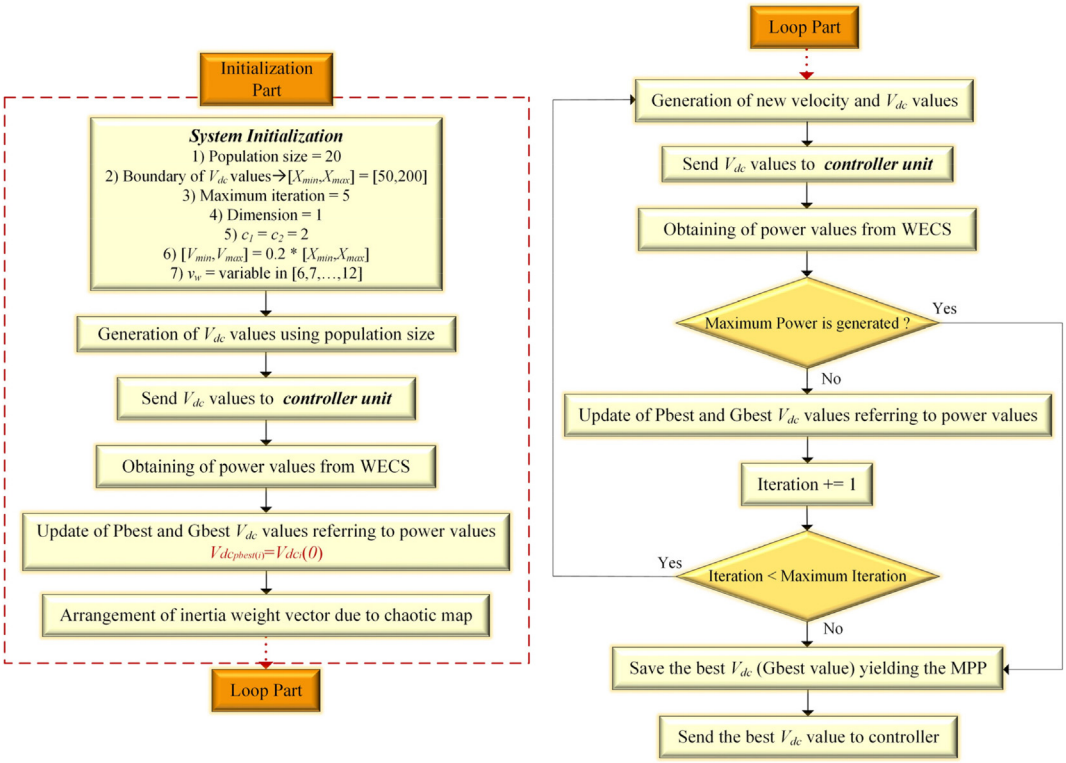

Fig. 4. Optimization part of hybrid framework.

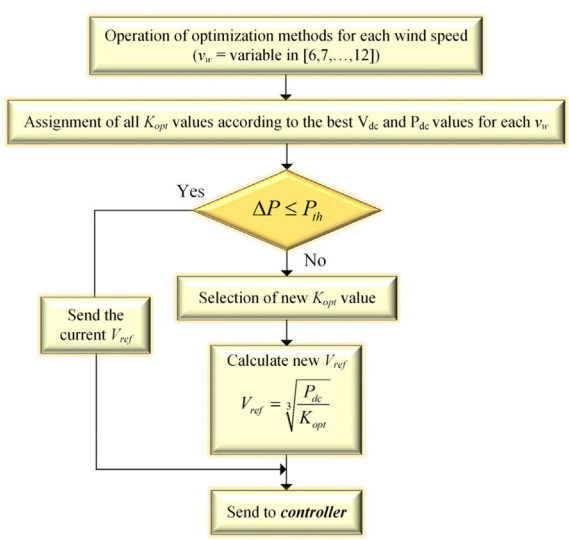

Fig. 5. ORB part of hybrid framework.

By replacing the state equations in (18) into (20), control signal is solved for $\dot{s} = 0$:

$$\dot{s} = -\frac{X_2}{RC} + \overline{u}\kappa\left(\frac{V_o - V_{in\_opt} + X_1}{LC}\right) + X_2\left(\alpha + \gamma\theta|X_1|^{\theta-1}\right) = 0$$
$$\mapsto u_{eq} = 1 + \frac{LC}{\kappa\left(V_o - V_{in\_opt} + X_1\right)} X_2\left(-\frac{1}{RC} + \alpha + \gamma\theta|X_1|^{\theta-1}\right) \tag{21}$$

Total control signal u_t consists of two parts and is supported by switching control signal as below:

$$u_t = u_{eq} + u_{sw},\ \{u_{sw} = K_{sw}\, sign(s)\} \tag{22}$$

where $K_{sw} > 0$ and $sign(.)$ denotes the signum function. u_{sw} tries to pull the system states to sliding manifold for $s(t) \neq 0$ and it is deactivated when the manifold is reached. The total control signal is as follows:

$$u_t = 1 + \frac{LC}{\kappa\left(V_o - V_{in\_opt} + X_1\right)} X_2\left(-\frac{1}{RC} + \alpha + \gamma\theta|X_1|^{\theta-1}\right) + K_{sw}\, sign(s) \tag{23}$$

4. Simulation results and discussions

This section presents all designs, validation tests and comparisons for proposed MPPT frameworks, TSR and ORB method, which are performed based on Matlab/Simulink simulation environment. Specifications for the wind turbine, PMSG parameters and BC parameters are given in Tables 1–3, respectively. Also, specifications for hybrid optimization algorithms are given in Table 4. Herein, three particular wind speed scenarios changing in the range from 6 m/s to 12 m/s are created for a comprehensive analysis. All MPPT methods are compared with each other in terms of some criteria such as efficiency, output power, output voltage, BC input voltage, C_P and duty ratio change. Moreover, the changes of K_{opt} coefficients for GM-CPSO and ORB MPPT and CDW-PSO and ORB MPPT methods are presented.

Table 1
Specifications for the wind turbine model.

Definition	Value
Air density	ρ_a = 1.225 kg/m^3
Optimal *TSR*	λ_{opt} = 8.1
Maximum power coefficient	C_{P_max} = 0.48
Pitch angle	β = 0
Rotor radius	R = 2
The coefficients C_1 to C_6	C_1 = 0.5176 C_2 = 116 C_3 = 0.4 C_4 = 5 C_5 = 21 C_6 = 0.0068

Table 2
PMSG parameters.

Definition	Value
Phase number	3
Rotor type	Salient-pole
Stator phase resistance	1 Ω
Armature inductance	L_d, L_q = 0.00153H
Inertia, J	0.013 $(kg.m^2)$
Viscous damping, F	0.0425 (N.m.s)
Pole pairs number n_p	16

Table 3
DC-DC boost converter parameters.

Definition	Value
Switching frequency, f_{sw}	5 kHz
Inductor, L	310 μH
Capacitor, C	240 μF
Inductor resistance, R_L	0.15 Ω
Capacitor ESR, R_C	0.07 Ω
Load resistance, R	36 Ω

Table 4
Specifications for hybrid optimization algorithms.

Definition	Value
Population size	20
Maximum iteration	5
Position limitations	$[X_{min},X_{max}]$ = [50,200]
Velocity limitations	$[V_{min},V_{max}] = 0.2*[X_{min},X_{max}]$
Dimension	1
Acceleration constants	$c_1 = c_2 = 2$

4.1. Test scenario I

The first scenario, in which the wind speed has step variations in the same range during the operation period, is indicated in Fig. 6. In this wind speed profile, the changes in operating voltages determined by four MPPT methods are shown in Fig. 7. Here, it can be seen that TSR method is far from the operating voltages found with the results attained by GM-CPSO and CDW-PSO methods, especially for high wind speed conditions. In addition, ORB is slightly closer to these optimal voltages than TSR. However, the best operating points are obtained based on optimization methods, and V_{in_best} & K_{opt} coefficients for the GM-CPSO and CDW-PSO are given in Table 5. Obviously, the extracted power provides close results, and the extracted output power graph is presented in Fig. 8. One can clearly observe that, GM-CPSO/ CDW-PSO and ORB MPPT methods yield higher power than ORB method and TSR method thanks to improvements in the MPPT accuracy,

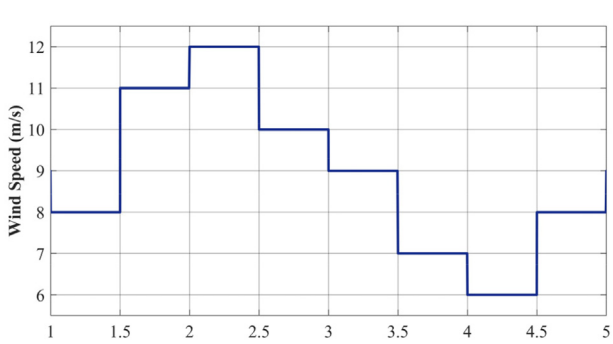

Fig. 6. Wind speed profile for test scenario I.

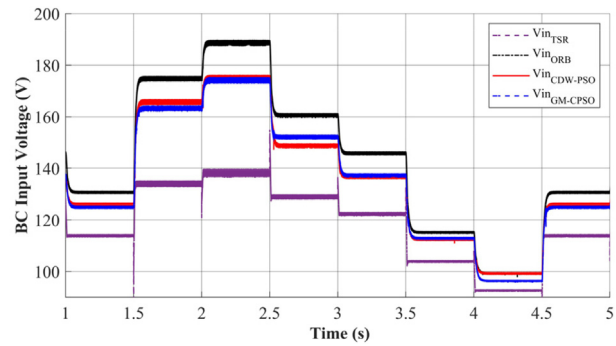

Fig. 7. Changes of BC input voltages for test scenario I.

namely more accurate and precise determination of the operating voltage points. For each wind speed, the data of the extracted power by four MPPT methods are indicated in Table 6. Also, the efficiency changing for the tested wind speeds is indicated in Fig. 9. In a similar way, it can be interpreted that the efficiency of TSR decreases as the wind speeds increase. The reason for this decrease is that the generator and converter losses are affected by the operation conditions because of the dependency of generator speed on wind speed and the losses change accordingly. For this reason, it cannot be so meaningful to keep C_P always at maximum value. For this wind speed profile, Fig. 10 presents the change of C_P corresponding to operation condition at which maximum power is achieved. On the other hand, the change of duty ratio generated by FTSMC MPPT controller is given in Fig. 11. The transitions between K_{opt} coefficients determined via optimization methods is also demonstrated in Fig. 12.

4.2. Test scenario II

To further verify the effectiveness, the second scenario is organized in the same wind speed range. However, slightly different from the first scenario, it is arranged as having both sudden steeply and linear changes with different slopes in the wind speed (Fig. 13). The performance evaluation of four MPPT methods is discussed in terms of BC input voltage, extracted output power, C_P, duty ratio and K_{opt} coefficients determined by optimization methods. In Fig. 14, the change of BC input voltages determined by MPPT methods is demonstrated. Besides, the change of output power extracted from WECS is indicated in Fig. 15. One can readily observe from Fig. 14 and Fig. 15 that the optimization based MPPT methods provide superior power extraction than the other methods. Herein, it can be revealed that the determined reference operating voltages are kept at the optimal value by improving the MPPT accuracy with the integration of the optimization methods. Additionally, TSR that is one of the conventional methods exhibits inferior performance than the others. Meanwhile, the variations of C_P for this wind speed profile are shown in Fig. 16. As seen in here, C_P is successfully kept at 0.48 in TSR method. However, as mentioned before, it can be understood from the obtained results that maximum power cannot be always achieved by keeping C_P at maximum value, and this deduction can be confirmed with Figs. 15 and 16. The data for the extracted average power, total energy and efficiency during the simulation time for four MPPT methods are given in Table 7. According to this table, the efficiency of hybrid GM-CPSO and ORB MPPT method can reach up to nearly 98.66%. On the other side, the changes of duty ratio produced via FTSMC MPPT controller is given in Fig. 17. Furthermore, the switching of K_{opt} coefficients for two optimization based methods is indicated in Fig. 18. Based on the switching, the transitions in reference

Table 5
The best values and coefficients obtained by optimization methods.

$V_w(m/s)$	CDW-PSO		GM-CPSO	
	V_{in_best} (V)	$K_{OPT}(\sim)$	V_{in_best} (V)	$K_{OPT}(\sim)$
6	100.3912	6.352159e-04	97.5444	6.921807e-04
7	113.6705	6.807221e-04	114.001	6.742761e-04
8	127.1802	7.087597e-04	126.1652	7.262426e-04
9	137.8511	7.718812e-04	138.5222	7.621728e-04
10	149.9471	7.993639e-04	153.3051	7.493665e-04
11	166.9165	7.493850e-04	164.500	7.840210e-04
12	176.1076	8.037671e-04	175.3568	8.148773e-04

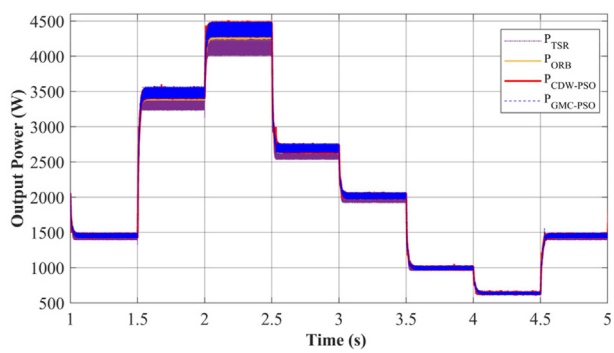

Fig. 8. Changes of output electrical power extracted from WECS for test scenario I.

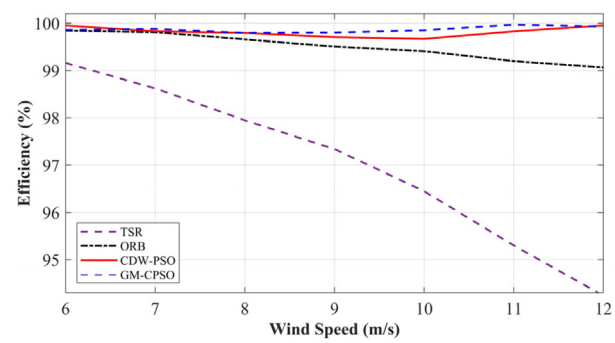

Fig. 9. Change of the efficiency for test scenario I.

operating voltages can be seen in Fig. 14 and in the meantime, this affects the duty ratio operation.

4.3. Test scenario III

As the nature of the wind is dynamic and having turbulence, the last scenario is created to evaluate and compare performance of four MPPT methods in the random wind speed varying between 7.5 m/s and 12 m/s, which is shown in Fig. 19. This wind speed profile with the medium turbulence has an average value of about 9.86 m/s. Herein, the critical evaluations on BC input voltage, extracted output power, C_P, duty ratio and K_{opt} coefficients variations have been made as similar to test scenario I and II. Figs. 20 and 21 demonstrate the changes of the BC input voltage, and the output electrical power extracted from WECS, respectively. It can be inferred from here that MPPT accuracy has been improved with the integration of the optimization methods. Thus, the reference operating voltages are determined more accurately. This makes a significant contribution to power extraction from WECS and also, superior results can be obtained by two optimization based MPPT methods for this test scenario. Besides, Table 8 provides the obtained data in terms of efficiency, extracted average power and total energy for four different MPPT methods. Herein, the efficiency of hybrid GM-CPSO based ORB MPPT method can reach up to about 98.60%. On the other hand, Fig. 22 indicates changes of the power

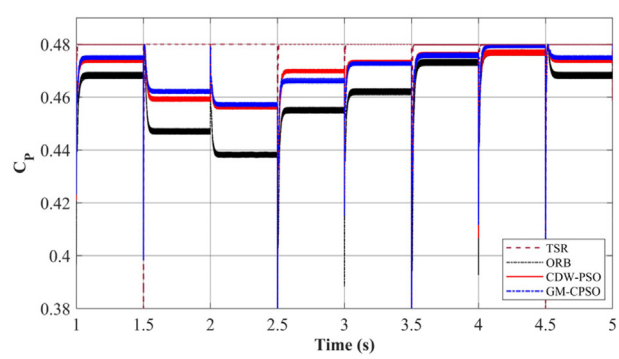

Fig. 10. Change of C_P values for test scenario I.

coefficients C_P for these four methods and C_P is maintained at 0.48 with TSR method. However, as mentioned in the previous sections, it can be enounced to be better for hybrid GM-CPSO based ORB and CDW-PSO based ORB MPPT methods because the extracted electrical power reaches their maximum for different values of C_P. On the other hand, the change of duty ratio for each method is presented in Fig. 23. It can be seen that for these optimization based methods, duty ratio is maintained in the range of 0.44–0.57 while is generally ranged between 0.40 and 0.65 for four methods. Also, Fig. 24

Table 6
Comparison of extracted power for MPPT methods for test scenario I.

V_w (m/s)	Available P_{max} (W)	P_{TSR} (W)	P_{ORB} (W)	$P_{CDW\text{-}PSO\text{-}ORB}$ (W)	$P_{GM\text{-}CPSO\text{-}ORB}$ (W)
6	643	637.6	642	**642.7**	642.1
7	1001	987.2	999.1	999.3	**999.8**
8	1461	1431	1456	**1458**	**1458**
9	2028	1974	2018	2022	**2024**
10	2703	2607	2687	2694	**2699**
11	3490	3327	3463	3485	**3490**
12	4392	4139	4351	**4390**	4389

Bold data indicates the highest value for each comparison. superior method is highlighted as bold.

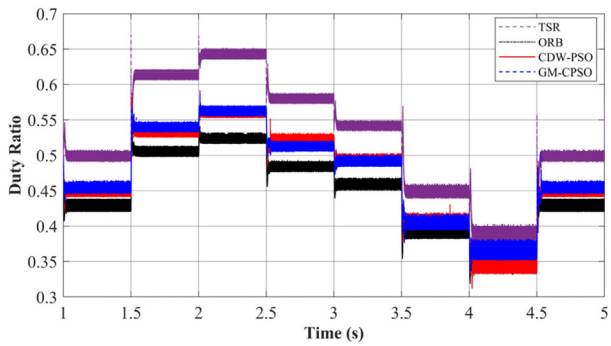

Fig. 11. Change of duty ratio for test scenario I.

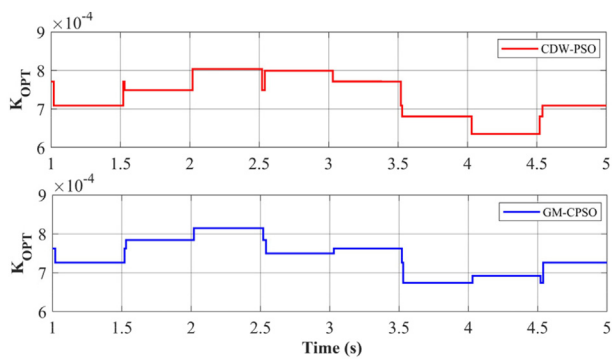

Fig. 12. Change of the K_{opt} coefficients for test scenario I.

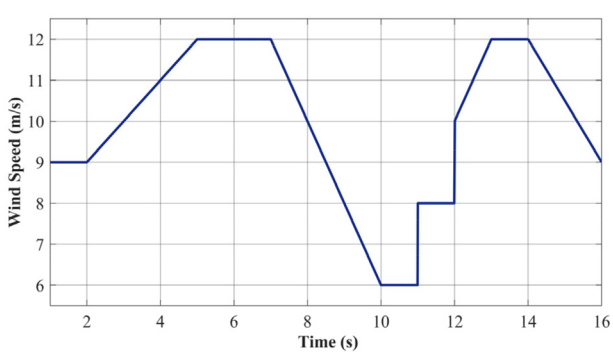

Fig. 13. Wind speed profile for test scenario II.

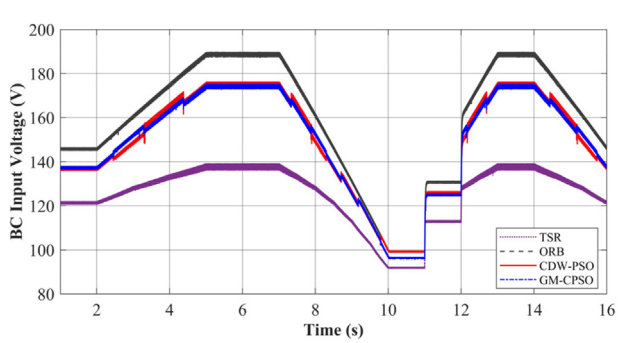

Fig. 14. Change of BC input voltages for test scenario II.

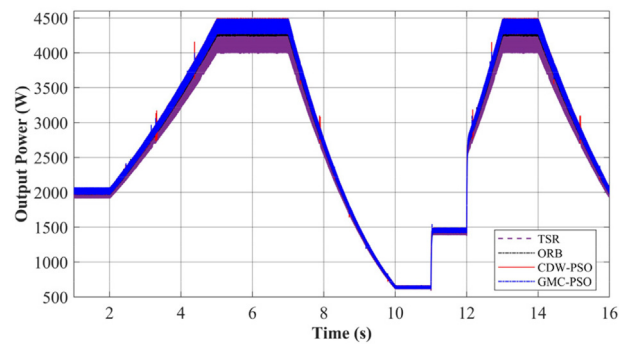

Fig. 15. The extracted output power from WECS for test scenario II.

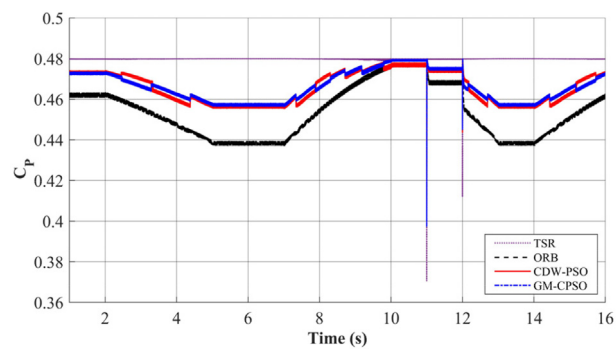

Fig. 16. Change of C_P values for test scenario II.

presents the switching of K_{opt} coefficients for two optimization based methods.

5. Conclusion

In this paper, a unified effective framework has been presented to maximize wind power extraction. This framework consists of fast terminal sliding mode based MPPT controller and two hybrid MPPT algorithms combining CDW-PSO and GM-CPSO techniques diversely with ORB MPPT method that has never been used in a WECS before. CDW-PSO and GM-CPSO have been used to find the optimum coefficients by searching the peak value of the maximum output power to be extracted. In order to ensure MPPT efficiency, these coefficients must be determined optimally to achieve the maximum power. After these algorithms generate the optimum coefficients, the framework passes to the second part in which ORB MPPT method is operated according to these coefficients. Moreover, this framework offers several advantages and it does not require any mechanical sensor and prior knowledge of the system. On the other hand, FTSMC is used to bring the system to optimum operating point determined by the proposed hybrid MPPT method. Three particular wind speed scenarios in the simulation environment are created to highlight the promising features of the proposed MPPT methods. Then, the proposed CDW-PSO based ORB and GMC-PSO based ORB MPPT methods are compared with conventional ORB and TSR methods in terms of maximum output power and MPPT efficiency. The findings of this study indicate that the proposed optimization based methods contribute to MPPT efficiency and reach superior wind power than the other conventional methods. Furthermore, the proposed combined framework has a relatively simple design and can be easily implemented in the actual WECS where system parameters are unknown. It should also be noted that the optimization manage-

Table 7
Comparison of the extracted powers by MPPT methods for test scenario II.

	Available	TSR	ORB	CDW-PSO-ORB	GM-CPSO-ORB
Average Power (W)	2902.62	2730.45	2846.98	2863.64	**2863.79**
Total Energy (W.s)	43539.34	40956.71	42704.74	42954.66	**42956.91**
Efficiency (%)	–	94.0685	98.0831	98.6571	**98.6622**

Bold data indicates the highest value for each comparison. superior method is highlighted as bold.

Table 8
Comparison of the extracted powers by MPPT methods for test scenario III.

	Available	TSR	ORB	CDW-PSO-ORB	GM-CPSO-ORB
Average Power (W)	2689.98	2547.02	2640.35	2651.13	**2652.22**
Total Energy (W.s)	80430.39	76155.99	78946.46	79268.80	**79301.37**
Efficiency (%)	–	94.6856	98.1550	98.5558	**98.5963**

Bold data indicates the highest value for each comparison. superior method is highlighted as bold.

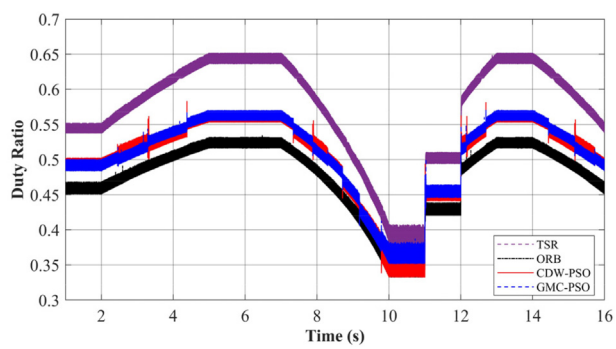

Fig. 17. Change of duty ratio for test scenario II.

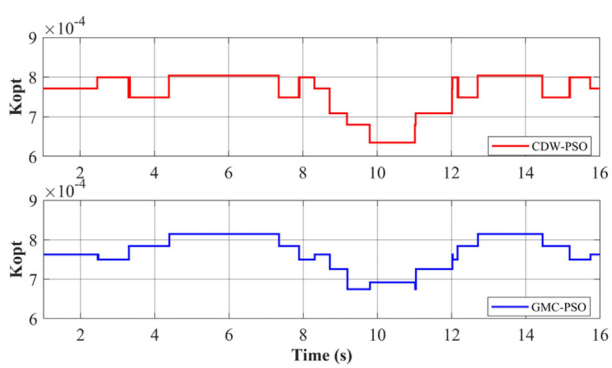

Fig. 18. Change of K_{opt} coefficients for test scenario II.

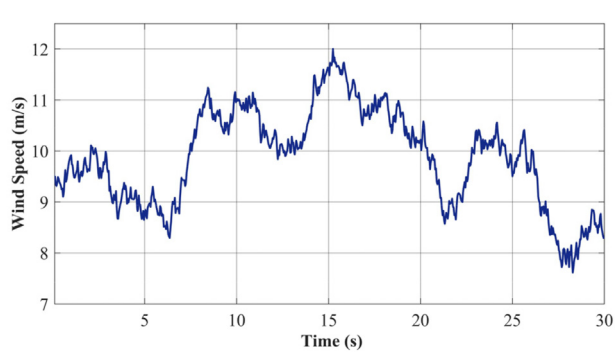

Fig. 19. Random wind speed profile for test scenario III.

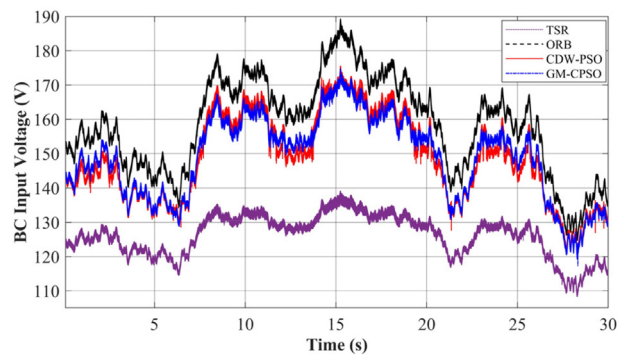

Fig. 20. Changes of BC input voltages for test scenario III.

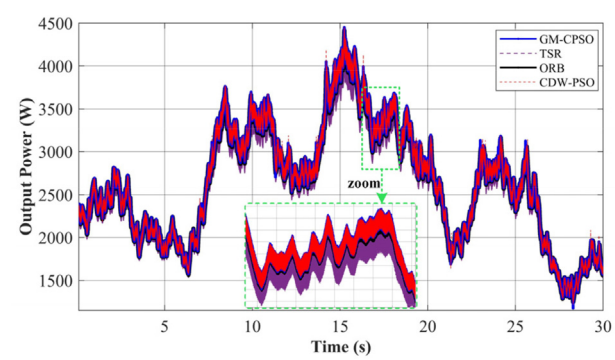

Fig. 21. The extracted output power from WECS for test scenario III.

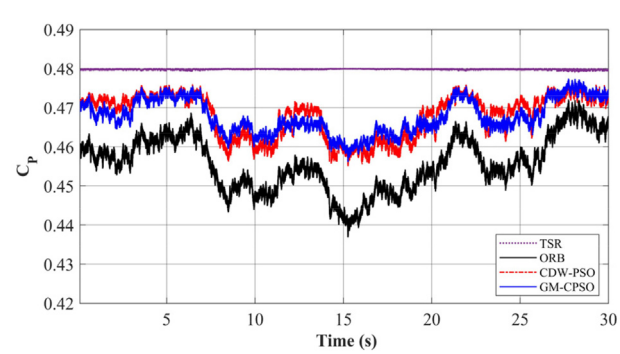

Fig. 22. Change of C_P values for test scenario III.

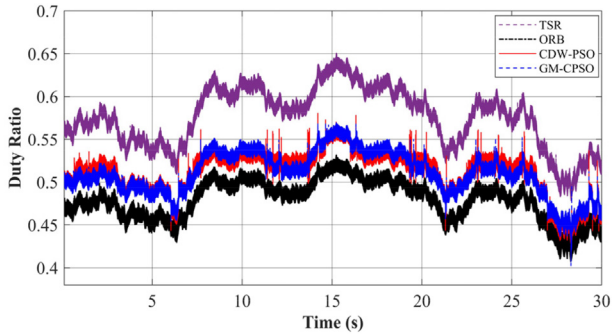

Fig. 23. Change of duty ratio for test scenario III.

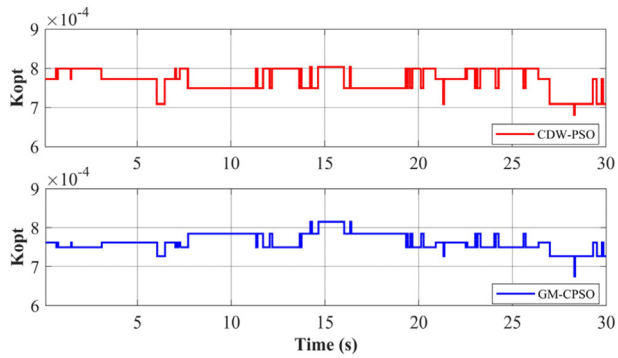

Fig. 24. Change of K_{opt} coefficients for test scenario III.

ment is considered as an off-line process in our study. Nonetheless, the MPPT operation is a completely online process. Since a limited part of this framework is carried out online, the overall processing load does not increase significantly. Further work could focus on different controller design methods and to the optimization of the parameters of these controllers. Also, we intend to develop the proposed frameworks and assess them on an experimental system in real-time.

Declaration of Competing Interest

The authors declare that they have no known competing financial interests or personal relationships that could have appeared to influence the work reported in this paper.

Acknowledgments

This work is supported by the Coordinatorship of Konya Technical University's Scientific Research Projects, and also, The Scientific and Technological Research Council of Turkey (TUBITAK) BIDEB-2211/C, Turkey.

References

[1] M.B.H. Kumar, B. Saravanan, P. Sanjeevikumar, F. Blaabjerg, Review on control techniques and methodologies for maximum power extraction from wind energy systems, IET Renewable Power Gener. 12 (2018) 1609–1622, https://doi.org/10.1049/iet-rpg.2018.5206.
[2] R. Sitharthan, M. Karthikeyan, D.S. Sundar, S. Rajasekaran, Adaptive hybrid intelligent MPPT controller to approximate effectual wind speed and optimal rotor speed of variable speed wind turbine, ISA Trans. 96 (2020) 479–489, https://doi.org/10.1016/j.isatra.2019.05.029.
[3] M.M. Hossain, M.H. Ali, Future research directions for the wind turbine generator system, Renewable Sustainable Energy Rev. 49 (2015) 481–489, https://doi.org/10.1016/j.rser.2015.04.126.
[4] M. Nasiri, J. Milimonfared, S.H. Fathi, Modeling, analysis and comparison of TSR and OTC methods for MPPT and power smoothing in permanent magnet synchronous generator-based wind turbines, Energy Convers. Manage. 86 (2014) 892–900, https://doi.org/10.1016/j.enconman.2014.06.055.
[5] Z.M. Dalala, Z.U. Zahid, W. Yu, Y. Cho, J. Lai, Design and analysis of an MPPT technique for small-scale wind energy conversion systems, IEEE Trans. Energy Convers. 28 (2013) 756–767, https://doi.org/10.1109/TEC.2013.2259627.
[6] X.-X. Yin, Y.-G. Lin, W. Li, Y.-J. Gu, P.-F. Lei, H.-W. Liu, Sliding mode voltage control strategy for capturing maximum wind energy based on fuzzy logic control, Int. J. Electr. Power Energy Syst. 70 (2015) 45–51, https://doi.org/10.1016/j.ijepes.2015.01.029.
[7] H.H.H. Mousa, A.-R. Youssef, E.E. Mohamed, Hybrid and adaptive sectors P&O MPPT algorithm based wind generation system, Renewable Energy 145 (2020) 1412–1429, https://doi.org/10.1016/j.renene.2019.06.078.
[8] D. Kumar, K. Chatterjee, A review of conventional and advanced MPPT algorithms for wind energy systems, Renewable Sustainable Energy Rev. 55 (2016) 957–970, https://doi.org/10.1016/j.rser.2015.11.013.
[9] E.J.N. Menezes, A.M. Araújo, N.S.B. Silva, A review on wind turbine control and its associated methods, J. Cleaner Prod. 174 (2018) 945–953, https://doi.org/10.1016/j.jclepro.2017.10.297.
[10] M.A. Abdullah, A.H.M. Yatim, C.W. Tan, R. Saidur, A review of maximum power point tracking algorithms for wind energy systems, Renewable Sustainable Energy Rev. 16 (2012) 3220–3227, https://doi.org/10.1016/j.rser.2012.02.016.
[11] J. Lee, Y. Kim, Sensorless fuzzy-logic-based maximum power point tracking control for a small-scale wind power generation systems with a switched-mode rectifier, IET Renewable Power Gener. 10 (2016) 194–202, https://doi.org/10.1049/iet-rpg.2015.0250.
[12] M. Zribi, M. Alrifai, M. Rayan, Sliding mode control of a variable- speed wind energy conversion system using a squirrel cage induction generator, Energies 10 (2017) 604, https://doi.org/10.3390/en10050604.
[13] B. Yang, L. Jiang, L. Wang, W. Yao, Q.H. Wu, Nonlinear maximum power point tracking control and modal analysis of DFIG based wind turbine, Int. J. Electr. Power Energy Syst. 74 (2016) 429–436, https://doi.org/10.1016/j.ijepes.2015.07.036.
[14] E.H. Dursun, A.A. Kulaksiz, in: in 3rd International Symposium on Multidisciplinary Studies and Innovative Technologies (ISMSIT), 2019, pp. 1–5, https://doi.org/10.1109/ISMSIT.2019.8932841.
[15] M.M. Bajestan, H. Madadi, M.A. Shamsinejad, Control of a new stand-alone wind turbine-based variable speed permanent magnet synchronous generator using quasi-Z-source inverter, Electr. Power Syst. Res. 177 (2019), https://doi.org/10.1016/j.epsr.2019.106010 106010.
[16] B. Yang, T. Yu, H. Shu, X. Zhang, K. Qu, L. Jiang, Democratic joint operations algorithm for optimal power extraction of PMSG based wind energy conversion system, Energy Convers. Manage. 159 (2018) 312–326, https://doi.org/10.1016/j.enconman.2017.12.090.
[17] Y. Mokhtari, D. Rekioua, High performance of Maximum Power Point Tracking Using Ant Colony algorithm in wind turbine, Renewable Energy 126 (2018) 1055–1063, https://doi.org/10.1016/j.renene.2018.03.049.
[18] B. Yang, L. Zhong, T. Yu, H. Shu, P. Cao, N. An, Y. Sang, L. Jiang, PCSMC design of permanent magnetic synchronous generator for maximum power point tracking, IET Gener. Transm. Distrib. 13 (2019) 3115–3126, https://doi.org/10.1049/iet-gtd.2018.5351.
[19] L. Wang, L. Cao, L. Zhao, Non-linear tip speed ratio cascade control for variable speed high power wind turbines: a backstepping approach, IET Renewable Power Gener. 12 (2018) 968–972, https://doi.org/10.1049/iet-rpg.2017.0698.
[20] B. Yang, T. Yu, H. Shu, Y. Zhang, J. Chen, Y. Sang, L. Jiang, Passivity-based sliding-mode control design for optimal power extraction of a PMSG based variable speed wind turbine, Renewable Energy 119 (2018) 577–589, https://doi.org/10.1016/j.renene.2017.12.047.
[21] L. Yang, J. Yang, Nonsingular fast terminal sliding-mode control for nonlinear dynamical systems, Int. J. Robust Nonlinear Control 21 (2011) 1865–1879, https://doi.org/10.1002/rnc.1666.
[22] M. Cheng, Y. Zhu, The state of the art of wind energy conversion systems and technologies: A review, Energy Convers. Manage. 88 (2014) 332–347, https://doi.org/10.1016/j.enconman.2014.08.037.
[23] M. Yin, W. Li, C.Y. Chung, L. Zhou, Z. Chen, Y. Zou, Optimal torque control based on effective tracking range for maximum power point tracking of wind turbines under varying wind conditions, IET Renewable Power Gener. 11 (2017) 501–510, https://doi.org/10.1049/iet-rpg.2016.0635.
[24] J. Castelló, J.M. Espí, R. García-Gil, Development details and performance assessment of a Wind Turbine Emulator, Renewable Energy 86 (2016) 848–857, https://doi.org/10.1016/j.renene.2015.09.010.
[25] M.A. Abdullah, T. Al-Hadhrami, C.W. Tan, A.H. Yatim, Towards green energy for smart cities: particle swarm optimization based MPPT approach, IEEE Access 6 (2018) 58427–58438, https://doi.org/10.1109/ACCESS.2018.2874525.
[26] H. Koyuncu, GM-CPSO: a new viewpoint to chaotic particle swarm optimization via gauss map, Neural Process. Lett. (2020), https://doi.org/10.1007/s11063-020-10247-2.
[27] H. Koyuncu, Parkinson's disease recognition using Gauss map based chaotic particle swarm–neural network, in: in 6th International Conference on Engineering and Telecommunication (En&T), 2019, pp. 1–4, https://doi.org/10.1109/EnT47717.2019.9030560.
[28] K. Chen, F. Zhou, A. Liu, Chaotic dynamic weight particle swarm optimization for numerical function optimization, Knowl.-Based Syst. 139 (2018) 23–40, https://doi.org/10.1016/j.knosys.2017.10.011.

[29] G.-G. Wang, L. Guo, A.H. Gandomi, G.-S. Hao, H. Wang, Chaotic Krill Herd algorithm, Inf. Sci. 274 (2014) 17–34, https://doi.org/10.1016/j.ins.2014.02.123.
[30] P. Niu, K. Chen, Y. Ma, X. Li, A. Liu, G. Li, Model turbine heat rate by fast learning network with tuning based on ameliorated krill herd algorithm, Knowl.-Based Syst. 118 (2017) 80–92, https://doi.org/10.1016/j.knosys.2016.11.011.
[31] R. Ceylan, H. Koyuncu, A novel rotation forest modality based on hybrid NNs, RF (ScPSO-NN), J. King Saud Univ.-Comput. Inf. Sci. 31 (2019) 235–251, https://doi.org/10.1016/j.jksuci.2017.10.011.
[32] S. Saremi, S. Mirjalili, A. Lewis, Biogeography-based optimisation with chaos, Neural Comp. Appl. 25 (2014) 1077–1097, https://doi.org/10.1007/s00521-014-1597-x.
[33] E.H. Dursun, A.A. Kulaksiz, MPPT control of PMSG based small-scale wind energy conversion system connected to DC-bus, Int. J. Emerging Electric Power Syst. (2020), https://doi.org/10.1515/ijeeps-2019-0188 20190188.
[34] S.M. Tripathi, A.N. Tiwari, D. Singh, Grid-integrated permanent magnet synchronous generator based wind energy conversion systems: a technology review, Renewable Sustainable Energy Rev. 51 (2015) 1288–1305, https://doi.org/10.1016/j.rser.2015.06.060.
[35] X. Zhang, Y. Zhang, S. Hao, L. Wu, W. Wei, An improved maximum power point tracking method based on decreasing torque gain for large scale wind turbines at low wind sites, Electr. Power Syst. Res. 176 (2019), https://doi.org/10.1016/j.epsr.2019.105942 105942.
[36] R. Wai, L. Shih, Design of voltage tracking control for DC–DC boost converter via total sliding-mode technique, IEEE Trans. Ind. Electron. 58 (2011) 2502–2511, https://doi.org/10.1109/TIE.2010.2066539.
[37] I. Yazici, E.K. Yaylaci, Fast and robust voltage control of DC–DC boost converter by using fast terminal sliding mode controller, IET Power Electron. 9 (2016) 120–125, https://doi.org/10.1049/iet-pel.2015.0008.
[38] E.H. Dursun, A.A. Kulaksiz, Second-order sliding mode voltage-regulator for improving MPPT efficiency of PMSG-based WECS, Int. J. Electr. Power Energy Syst. 121 (2020), https://doi.org/10.1016/j.ijepes.2020.106149.
[39] X. Yu, M. Zhihong, Fast terminal sliding-mode control design for nonlinear dynamical systems, IEEE Trans. Circuits Syst. I: Fundam. Theory Appl. 49 (2002) 261–264, https://doi.org/10.1109/81.983876.